Pertanika J. Sci. & Technol. 34 (5): 2739 - 2763 (2026)

PERTANIKA JOURNALS

SCIENCE & TECHNOLOGY

Journal homepage: http://www.pertanika.upm.edu.my/

Regenerative Braking-Based Energy Recovery for Electric Motorcycles in Hilly Terrain

Mawada Ahmed[1], Siti Fauziah Toha[1]*, Khairul Affendy[1], Muhammad Abdullah[2], Salmiah Ahmad[3], Mohammad Osman Tokhi[4], and Ahmad Syahrin Idris[5]

[1]Department of Mechatronics Engineering, Kulliyyah of Engineering, International Islamic University Malaysia, Jalan Gombak, 53100 Gombak, Selangor, Malaysia
[2]Department of Mechanical and Aerospace Engineering, Kulliyyah of Engineering, International Islamic University Malaysia, Jalan Gombak, 53100 Gombak, Selangor, Malaysia
[3]College of Engineering and Technology, University of Doha for Science and Technology, Al Tarafa, Jelaiah Street, Duhail North, P.O. Box 24449, Doha, Qatar
[4]School of Engineering, London South Bank University, 103 Borough Road, London SE1 0AA, United Kingdom
[5]Department of Electrical and Electronic Engineering, University of Southampton Malaysia, 79100 Iskandar Puteri, Johor, Malaysia

ABSTRACT

Limited battery energy availability remains a major challenge for electric motorcycles, especially in hilly terrain, where repeated climbing and downhill braking increase variability in energy consumption. This study investigates regenerative braking as an energy-recovery strategy for an electric motorcycle using a MATLAB/Simulink-based model. The proposed model integrates longitudinal vehicle dynamics, road-gradient effects, an H-bridge inverter, an L-C filter, a DC machine, a lithium-ion battery, and feedforward/PID control strategies. The Worldwide Motorcycle Test Cycle (WMTC) was used as the reference speed profile to evaluate speed tracking, motor response, battery behaviour, recovered energy, and state of charge (SOC) variation. The results show that downhill operation creates suitable conditions for regenerative braking, allowing the electric machine to operate as a generator and return energy to the battery. Compared with feedforward control, the PID controller improved the simulated regenerative braking response by reducing the RMSE from 14.10 m/s to 11.546 m/s. The recovered energy increased from 1.00×10^5 J to 2.20×10^5 J, while the SOC variation improved from −13.0% to −10.2%. The SOC response also showed a temporary recovery

ARTICLE INFO

Article history:
Received: 04 June 2026
Accepted: 26 August 2026
Published: 30 October 2026

DOI: https://doi.org/10.47836/pjst.34.5.09

E-mail addresses:
Mawadaahmed184@gmail.com (Mawada Ahmed)
tsfauziah@iium.edu.my (Siti Fauziah Toha)
mohd_abdl@iium.edu.my (Muhammad Abdullah)
salmiah.ahmad@udst.edu.qa (Salmiah Ahmad)
affendy@iium.edu.my (Khairul Affendy)
tokhim@lsbu.ac.uk (Mohammad Osman Tokhi)
A.S.Idris@soton.ac.uk (Ahmad Syahrin Idris)
* Corresponding author

e-ISSN: 2231-8526

© Universiti Putra Malaysia Press

during braking, confirming that part of the mechanical energy was returned to the battery. The battery current and power responses verified reversed energy flow during regeneration, while the torque response confirmed generator operation. Overall, the findings demonstrate that regenerative braking with PID control can improve energy recovery and reduce battery depletion in electric motorcycles operating in hilly terrain.

Keywords: Battery state of charge, electric motorcycle, energy recovery, hilly terrain, MATLAB/Simulink, PID control, regenerative braking system, WMTC

INTRODUCTION

Electric motorcycles (EMs) are increasingly important in the transition toward sustainable and energy-efficient transportation. Compared with conventional internal combustion engine motorcycles, EMs produce lower local emissions, generate less noise, have simpler drivetrain structures, and offer lower operating costs. The global shift toward electric vehicles (EVs) is driven by environmental concerns, fossil-fuel depletion, and the need to reduce carbon dioxide emissions from the transportation sector. Recent developments in battery technology, power electronics, electric machines, charging infrastructure, and energy management have further supported the growth of EV systems (International Energy Agency, 2022; Madichetty et al., 2021). Karyatanti et al. (2025) also emphasised that EV adoption can reduce air pollution, greenhouse gas emissions, and dependence on petroleum-based fuels.

Despite these advantages, limited driving range remains a major barrier to wider adoption of EVs and EMs. This limitation is mainly caused by limited battery capacity, long charging times, battery ageing, and varying power demands under real driving conditions. The issue is more critical for electric motorcycles because their compact design limits the space available for large battery packs. Therefore, improving onboard energy utilisation is essential, especially for lightweight vehicles operating in areas with limited charging infrastructure or challenging road profiles (Aduama et al., 2023; Kadav & Asher, 2019; Yang, 2022).

Hilly terrain represents a demanding operating condition for electric motorcycles. During uphill motion, additional energy is required to overcome gravitational resistance and maintain the desired speed. During downhill motion, some of the energy previously expended during climbing is again available as potential and kinetic energy. In conventional braking systems, this energy is dissipated as heat through friction brakes. Regenerative braking systems (RBSs) offer a practical method for recovering part of this energy by allowing the electric machine to operate as a generator during braking or downhill descent. The recovered electrical energy can then be returned to the battery, improving energy utilisation and reducing battery energy depletion. For two-wheeled vehicles, this

is especially relevant because lightweight design and efficient energy use are essential for operation on hilly roads (Nama et al., 2022; Rego & Castro, 2023).

Regenerative braking performance depends on several factors, including machine characteristics, inverter switching, braking control, road gradient, battery condition, and energy storage capability. Joseph Godfrey and Sankaranarayanan (2018) showed that braking mode selection and switching strategy affect the amount of recovered energy in BLDC motor-driven EVs. Heydari et al. (2019) demonstrated that energy recovery can be improved by dynamically adjusting the low-speed cutoff point, while Heydari et al. (2020) showed that optimal brake allocation can increase harvested braking energy. Other studies have investigated regenerative energy recovery through switched-capacitor voltage control, low-speed battery charging, and hybrid energy storage systems (Jung & Ko, 2021; Naseri et al., 2017; Podder et al., 2021; Yeo et al., 2020). These studies confirm that effective regenerative braking requires proper coordination between the motor, power electronics, control strategy, and battery system.

Regenerative braking has also been examined in terms of braking-force distribution and battery state-of-charge (SOC) performance. Ghazali et al. (2020) reported that regenerative braking is an energy-saving solution because conventional braking produces unnecessary heat losses, while RBS technology enables part of the braking energy to be recovered. Their study also highlighted that braking force distribution, SOC, motor performance, and overall vehicle performance must be considered together when designing an RBS. This is highly relevant to the present study because the proposed EM model evaluates regenerative braking not only through recovered energy but also through motor response and SOC behaviour during hilly-terrain operation.

Battery behaviour is also central to regenerative braking performance. The recovered energy is useful only if the battery can safely receive and store the regenerated current. Badran and Toha (2024) explained that lithium-ion batteries are widely used in EV applications due to their high energy density and long lifespan, but their performance depends on stability, efficiency, life cycle, SOC estimation, fault detection, and cell balancing. Similarly, studies on battery cooling, cell balancing, and energy storage management show that battery condition directly affects EV range and long-term performance (Riczu & Bauman, 2021; Xie et al., 2020). Therefore, state of charge (SOC), battery current, and battery voltage are important indicators when evaluating regenerative braking systems.

Several studies have examined regenerative braking with respect to braking-force distribution, battery SOC, and overall EV performance. Ghazali et al. (2020) reported that regenerative braking reduces energy loss from conventional friction braking and improves battery SOC by recovering braking energy. Their work also highlighted the need to consider the distribution of braking force, motor response, SOC, and vehicle performance together when designing an RBS. This supports the need for a coupled mechanical-electrical model

capable of evaluating vehicle motion, motor-generator operation, and battery response within a single simulation framework.

Electric motorcycles require dedicated modelling because their dynamics, packaging constraints, and energy capacity differ from those of four-wheeled EVs (Madichetty et al., 2021). The selection of the electric motor affects propulsion efficiency and vehicle performance. Rego and Castro (2023) showed that regenerative braking in electric motorcycle prototypes requires attention to vehicle-specific dynamics and energy recovery limits. Nama et al. (2022) further demonstrated the design, modelling, and hardware implementation of regenerative braking for electric two-wheelers on hilly roads. These studies show that motorcycle-specific regenerative braking models should include longitudinal dynamics, road-gradient effects, braking force, motor operation, and battery SOC response.

The present work also builds on previous studies related to lightweight electric mobility and electric drive systems. Mohamed et al. (2025) developed a smart IoT-based energy optimisation and localisation monitoring system for e-bike sharing, showing the importance of energy-aware monitoring in electric two-wheeler applications. Mohamed et al. (2025) investigated voltage regulation of buck converter-fed DC motors under dynamic load conditions, which is relevant to stable motor-drive operation under changing electrical and mechanical loads. These studies support the broader need for reliable energy management and controlled motor-drive behaviour in compact electric mobility systems.

Although regenerative braking has been widely studied in electric cars, hybrid vehicles, buses, rail systems, and charging infrastructure, fewer studies focus on electric motorcycles operating in hilly terrain. This gap is important because hilly routes involve repeated high-energy demands during climbs and repeated recovery opportunities during descents. A simplified and practical simulation framework is therefore needed to evaluate how regenerative braking can improve SOC behaviour and energy recovery in electric motorcycles under gradient-rich operating conditions.

Therefore, this paper investigates regenerative braking as an energy-recovery strategy for electric motorcycles operating in hilly terrain. A MATLAB/Simulink model is developed to link motorcycle longitudinal dynamics, road-gradient effects, braking force, motor-generator operation, H-bridge switching, battery current, voltage, SOC, and recovered energy. The study evaluates a practical regenerative braking configuration using feedforward and PID control strategies. The main contribution of this work is a coupled mechanical-electrical simulation framework that assesses whether regenerative braking can recover useful downhill energy, reduce battery depletion, and improve the energy performance of electric motorcycles in hilly environments.

MATERIALS AND METHODS

Research Design

This study used a MATLAB/Simulink-based modelling approach to evaluate regenerative braking as an energy-recovery strategy for an electric motorcycle operating in hilly terrain. The model integrates motorcycle longitudinal dynamics, a lithium-ion battery, an H-bridge inverter, an L-C filter, a DC machine, switching logic, and performance measurement blocks within a single simulation environment. The main purpose of the model is to analyse the transition between motoring and regenerative braking modes and to evaluate the electrical energy recovered during deceleration.

The scope of the study was limited to regenerative energy recovery, battery state-of-charge behaviour, speed-tracking response, and energy-flow direction. Direct driving-range estimation, no-regeneration baseline comparison, and hardware-level component sizing were not included in the present model.

The overall structure of the proposed regenerative braking system for electric motorcycles is shown in Figure 1. The model receives the Worldwide Motorcycle Test Cycle (WMTC) as the reference speed input. The vehicle dynamics subsystem calculates the force demand, torque, angular speed, and mechanical power. The battery supplies energy during motoring mode and receives energy during regenerative braking mode. The H-bridge inverter controls the current direction through four MOSFET switches, while the L-C filter reduces switching ripple. The performance-output block calculates speed, torque, braking force, electrical power, mechanical power, recovered energy, and efficiency.

The operating principle of the electric motorcycle is shown in Figure 2. During motoring mode, electrical energy flows from the battery to the motor, which produces driving torque.

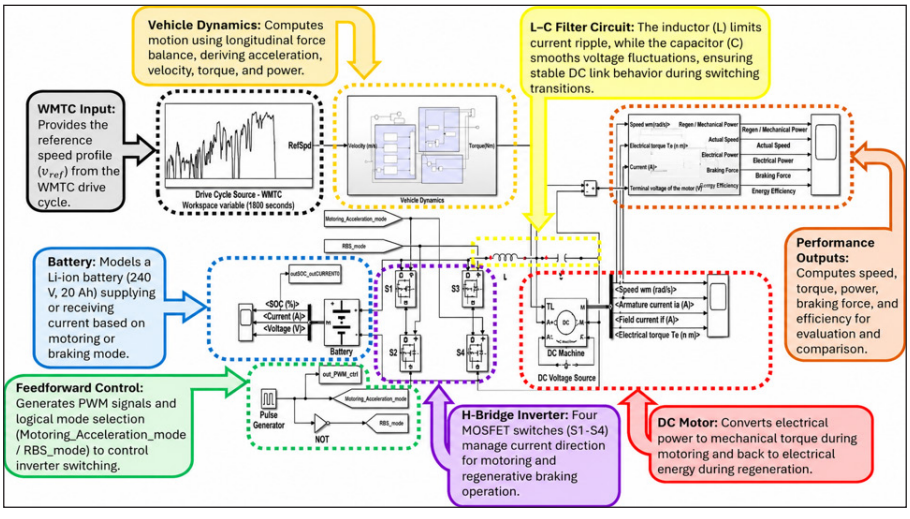

Figure 1. Overall MATLAB/Simulink architecture of the electric motorcycle regenerative braking system

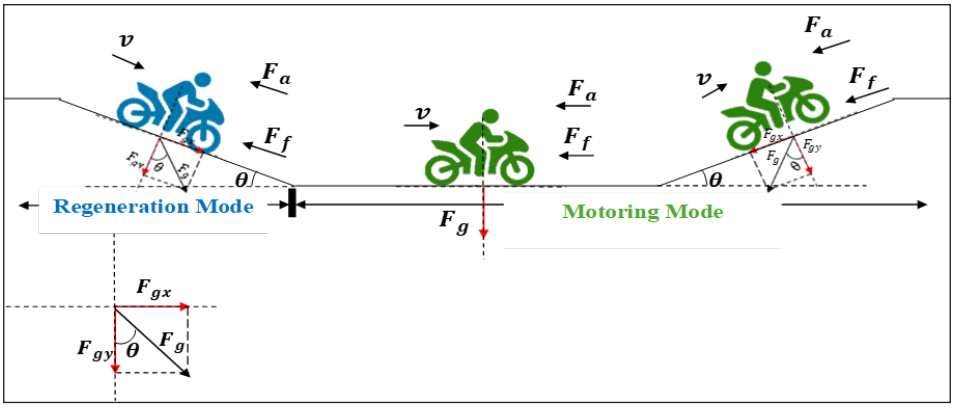

Figure 2. Operating principle of the electric motorcycle during motoring and regenerative braking modes

During regenerative braking mode, the wheel drives the machine mechanically, causing it to operate as a generator. In this condition, part of the mechanical energy is converted into electrical energy and returned to the battery.

Electric Motorcycle Model Parameters

The electric motorcycle was represented as a longitudinal single-track vehicle. The model focuses on straight-line motion, road-gradient effects, braking force, wheel torque, motor operation, and energy recovery. Lateral dynamics, steering behaviour, tyre slip, rider posture variation, and detailed mechanical brake blending were not considered, since the main purpose of this study is to analyse regenerative braking energy flow.

All vehicle-dynamics equations were defined using SI units. The vehicle speed, wheel angular speed, force, torque, and power variables were treated consistently according to the longitudinal vehicle model. A direct wheel-to-machine speed relationship was assumed through $v = r\omega$, and no separate gear ratio, transmission loss model, or detailed drivetrain efficiency map was included.

The parameters used in the longitudinal dynamics model are listed in Table 1. These parameters were used to calculate rolling resistance, aerodynamic drag, gradient resistance, inertial force, wheel torque, angular speed, and mechanical power.

Longitudinal Vehicle Dynamics

The longitudinal motion of the electric motorcycle was described using the force balance along the direction of travel. The model includes rolling resistance, aerodynamic drag, gradient resistance, and inertial force. These force components determine the total force demand at the wheel and are then used to calculate wheel torque and mechanical power.

Table 1
Motorcycle and Simulation Parameters Used in the Longitudinal Dynamics Model

Parameter	Symbol	Value	Unit	Description
Total mass, vehicle and rider	m	255	kg	Combined mass of the electric motorcycle and rider
Gravitational acceleration	g	9.81	m/s²	Standard gravitational acceleration
Wheel radius	r	0.30	m	Tyre rolling radius
Air density	ρ	1.18	kg/m³	Ambient air density
Frontal area	A	0.60	m²	Projected frontal area of the motorcycle
Aerodynamic drag coefficient	C_d	0.90	–	Coefficient representing aerodynamic resistance
Rolling resistance coefficient	μ_{rr}	0.01	–	Coefficient representing tyre-road rolling resistance
Rotational inertia coefficient	λ	1.03	–	Correction factor for wheel and drivetrain rotational inertia
Road angle	α	Variable	°	Road-gradient condition for flat, uphill, and downhill operation
Desired braking deceleration	a_{brake}	−15	m/s²	Target deceleration during braking mode
Initial angular speed	ω_0	300-400	rad/s	Initial wheel angular speed range
Simulation step size	T_s	0.1	s	Sampling time used for drive-cycle tracking
Drive cycle	–	WMTC	–	Worldwide Motorcycle Test Cycle reference speed profile
Drive-cycle duration	T	1800	s	Total duration of the WMTC profile

The rolling resistance force was calculated using Equation 1:

$$F_{rr} = mg\mu_{rr}cos(\alpha) \quad [1]$$

where F_{rr} is the rolling resistance force, m is the total motorcycle-rider mass, g is the gravitational acceleration, μ_{rr} is the rolling resistance coefficient, and α is the road angle.

The aerodynamic drag force was calculated using Equation 2:

$$F_{ad} = \frac{1}{2}\rho C_d A v^2 \quad [2]$$

where F_{ad} is the aerodynamic drag force, ρ is the air density, C_d is the aerodynamic drag coefficient, A is the frontal area, and v is the motorcycle speed.

The gradient resistance force was calculated using Equation 3:

$$F_g = mgsin(\alpha) \quad [3]$$

where F_g is the component of the gravitational force acting along the slope. During uphill motion, this force increases the required tractive effort. During downhill motion, it assists the motorcycle's motion and creates an opportunity for regenerative braking.

The inertial force was calculated using Equation 4:

$$F_i = \lambda m \frac{dv}{dt} \quad [4]$$

where F_i is the inertial force, λ is the rotational inertia coefficient, and dv/dt is the longitudinal acceleration.

The total longitudinal force was then obtained using Equation 5:

$$F_{total} = F_{rr} + F_{ad} + F_g + F_i \quad [5]$$

The required wheel torque was calculated using Equation 6:

$$T_W = F_{total}\, r \quad [6]$$

where T_W is the wheel torque and r is the wheel radius.

The relationship between motorcycle speed and wheel angular speed was calculated using Equation 7:

$$v = r\omega \quad [7]$$

where ω is the wheel angular speed.

The mechanical power at the wheel was calculated using Equation 8:

$$P_{mech} = T_w \omega \quad [8]$$

The mechanical variables calculated in the longitudinal subsystem represent the vehicle-side force, torque, angular speed, and power demand used to evaluate the simulated regenerative braking response. These variables were not intended to represent experimentally validated motor-shaft limits. The Simulink implementation of the vehicle dynamics subsystem is shown in Figure 3. The subsystem calculates rolling resistance, aerodynamic drag, gradient resistance, acceleration resistance, total force, wheel torque, and mechanical power.

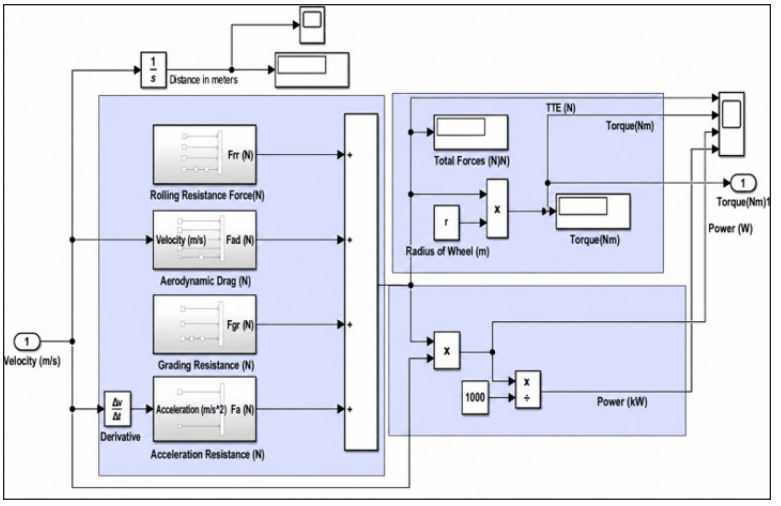

Figure 3. Vehicle dynamics subsystem for calculating force, torque, and mechanical power

Regenerative Braking System Architecture

The regenerative braking system was designed using a battery, an H-bridge inverter, an L-C filter, and a DC machine. The H-bridge inverter consists of four MOSFET switches that control the direction of current flow. During motoring mode, the battery supplies electrical energy to the DC machine. During regenerative braking mode, the DC machine operates as a generator, returning electrical energy to the battery.

The block-level structure of the regenerative braking system is shown in Figure 4. The controller selects either motoring or regenerative braking depending on the speed condition and braking demand. This selected mode controls the inverter switching state and determines whether electrical power flows from the battery to the motor or from the motor back to the battery.

The electrical and switching parameters used in the regenerative braking model are listed in Table 2.

The DC machine rating in Table 2 represents the nominal motor-generator parameter used in the model. The present work does not include detailed component-level saturation, torque-speed envelope limits, current protection limits, thermal constraints, battery charge-acceptance limits, or hardware derating. Therefore, the electrical and mechanical waveforms are interpreted as simulated response indicators for regenerative braking behaviour and controller comparison rather than final hardware operating ratings. Detailed component sizing and experimentally validated operating limits are recommended for future work. The detailed Simulink circuit of the regenerative braking model is shown in Figure 5. The circuit contains the battery, four MOSFET switches, an L-C filter, a DC voltage source, and a DC machine. The L-C filter is placed between the inverter and the machine side to reduce current ripple and smooth voltage fluctuation during switching.

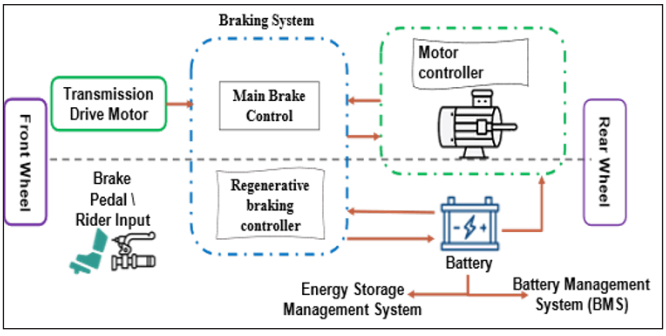

Figure 4. Block diagram of the regenerative braking system for the electric motorcycle drive

Table 2
Electrical and Switching Parameters of the Regenerative Braking Model

Component	Parameter	Symbol	Value	Unit	Description
Battery	Initial state of charge	SOC_0	50	%	Initial battery charge level
Battery	Battery type	–	Lithium-ion	–	Main energy source and storage element
DC machine	Rated power	P_m	5	HP	Motor-generator power rating
DC machine	Rated voltage	V_m	240	V	Rated machine voltage
DC machine	Rated speed	n_m	1750	rpm	Rated machine speed
DC voltage source	Source voltage	V_{dc}	300	V	DC supply voltage used in the circuit
Inductor	Inductance	L	5	mH	Limits current ripple
Capacitor	Capacitance	C	150	μF	Smooths DC-link voltage fluctuation
MOSFET bridge	Power switches	$S_1 - S_4$	4	–	Switches used for motoring and regeneration
Pulse generator	Time period	T_P	2×10^{-5}	s	Corresponds to 50 kHz switching frequency
Pulse generator	Pulse width	D	25	%	Switch-on duration within one PWM period

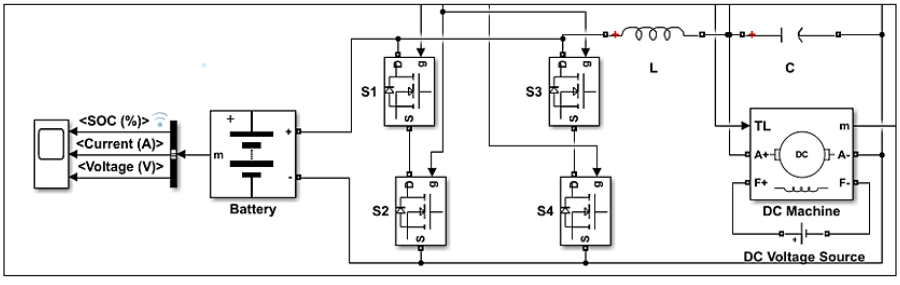

Figure 5. MATLAB/Simulink regenerative braking circuit with H-bridge inverter, L-C filter, battery, and DC machine

Motoring and Regenerative Braking Modes

The H-bridge inverter was controlled in two modes: motoring and regenerative braking. In motoring mode, the battery discharges and supplies current to the DC machine, enabling it to produce driving torque. In regenerative braking mode, the wheel drives the DC machine, and the generated electrical energy is directed back to the battery.

The switching states used in the H-bridge inverter are shown in Table 3. In motoring mode, switches S_1 and S_4 are turned ON, while S_2 and S_3 are turned OFF. In regenerative braking mode, switches S_2 and S_3 are turned ON, while S_1 and S_4 are turned OFF.

The current path during motoring mode is shown in Figure 6(a), while the current path during regenerative braking mode is shown in Figure 6(b). These figures show how the active switch pair changes the current direction and changes the DC machine operation between motor and generator modes.

Table 3
H-Bridge Switching States During Motoring and Regenerative Braking

Operating mode	S1	S2	S3	S4	Machine operation	Battery operation
Motoring mode	ON	OFF	OFF	ON	Motor	Discharging
Regenerative braking mode	OFF	ON	ON	OFF	Generator	Charging

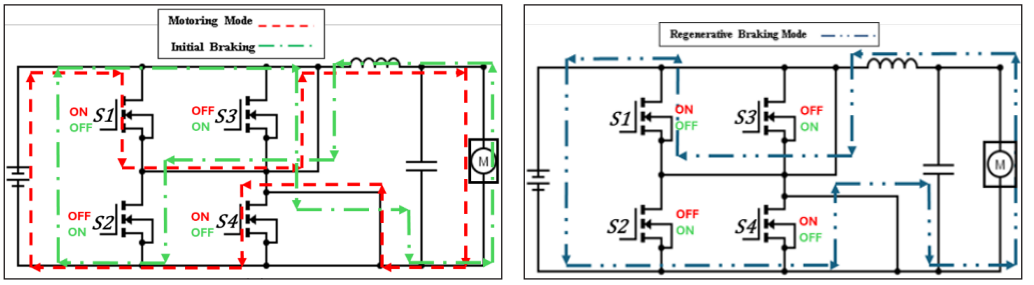

(a) (b)

Figure 6. H-bridge current paths: (a) motoring mode and (b) regenerative braking mode

Mode Selection Logic

The operating mode was selected using switching logic based on braking demand and the relationship between the reference speed and the actual speed. The reference speed was obtained from the WMTC drive-cycle profile, while the actual speed was calculated from the vehicle dynamics subsystem.

The speed error was calculated using Equation 9:

$$e(t) = v_{ref}(t) - v(t) \quad [9]$$

where $e(t)$ is the speed error, $v_{ref}(t)$ is the reference speed, and $v(t)$ is the actual motorcycle speed.

Regenerative braking was activated when the actual speed exceeded the reference speed or when braking input was applied. The speed-based switching condition is shown in Equation 10:

$$v(t) > v_{ref}(t) \quad [10]$$

When Equation 10 is satisfied, the inverter switches from motoring mode to regenerative braking mode. This allows the DC machine to generate opposing torque and return current to the battery.

The complete mode-selection process is shown in Figure 7. The process begins with rider or brake-pedal input. The system then checks whether the electric motorcycle is active and selects either motoring mode or regenerative braking mode by activating the corresponding switch pair.

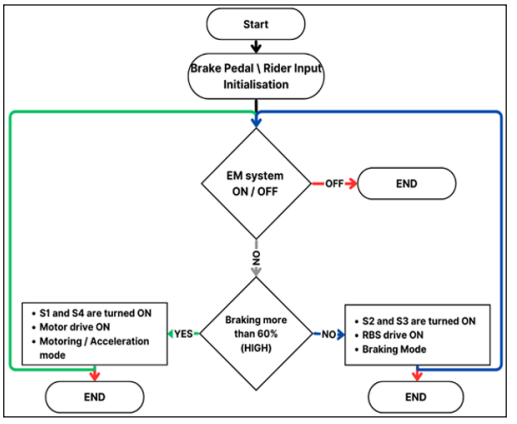

Figure 7. Flowchart of the motoring and regenerative braking mode-selection process

Feedforward and PID Control

A feedforward command was used to provide the initial switching and PWM signal based on the reference drive-cycle condition. The feedforward signal was defined as a function of the reference speed and reference acceleration, as shown in Equation 11:

$$u_{ff}(t) = f(v_{ref}(t), a_{ref}(t)) \quad [11]$$

where $u_{ff}(t)$ is the feedforward command, $v_{ref}(t)$ is the reference speed, and $a_{ref}(t)$ is the reference acceleration obtained from the WMTC profile.

A PID controller was used to improve speed-tracking response by adjusting the duty cycle based on the difference between the reference and actual speeds. The PID control signal was calculated using Equation 12:

$$u_{PID}(t) = K_p e(t) + K_i \int e(t)dt + K_d \frac{de(t)}{dt} \quad [12]$$

where $u_{PID}(t)$ is the PID output, K_p is the proportional gain, K_i is the integral gain, K_d is the derivative gain, and $e(t)$ is the speed error.

The PWM duty cycle was limited using Equation 13.

$$0 \leq D(t) \leq 1 \quad [13]$$

where $D(t)$ is the inverter duty cycle.

The PID-based Simulink implementation is shown in Figure 8. The WMTC reference speed is compared with the actual motorcycle speed, and the PID controller generates the duty-cycle correction signal. The corrected PWM signal is then applied to the H-bridge inverter to improve speed tracking and regulate regenerative braking.

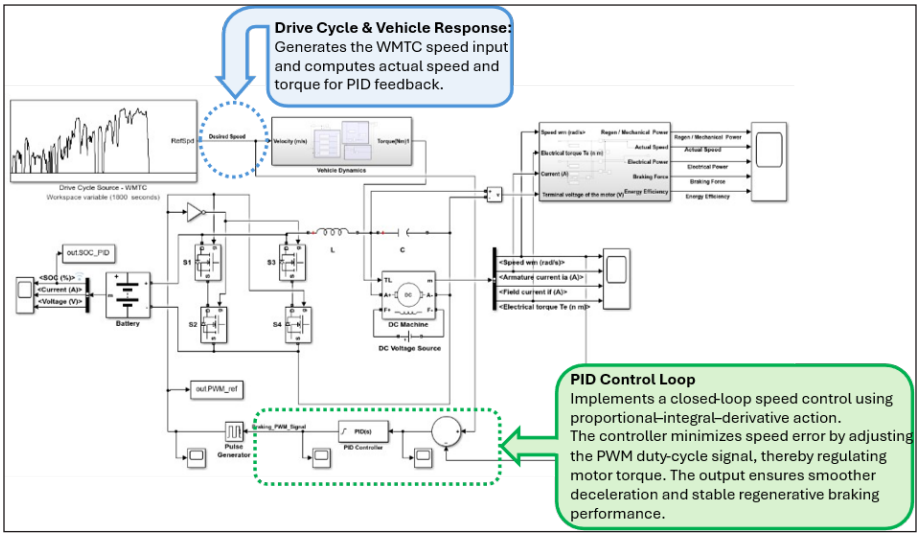

Figure 8. PID-based Simulink control structure for regenerative braking

Battery Model and Energy Flow Calculation

The lithium-ion battery was modelled as the main energy source during motoring and as the storage element during regenerative braking. During motoring, the battery current is positive because electrical energy flows from the battery to the motor. During regenerative braking, the battery current becomes negative because electrical energy flows from the generator back to the battery. The battery voltage, current, power, and SOC were recorded to evaluate the system's charging and discharging behaviour.

The instantaneous battery power was calculated using Equation 14:

$$P_{batt}(t) = V_{batt(t)}\, I_{batt(t)} \quad [14]$$

where $P_{batt(t)}$ is the battery power, $V_{batt(t)}$ is the battery terminal voltage, and $I_{batt(t)}$ is the battery current.

The recovered regenerative energy was calculated by integrating the charging portion of the battery power curve, as shown in Equation 15:

$$E_{regen} = \int_0^T max\,(0, -P_{batt}\,(t))dt \quad [15]$$

where E_{regen} is the recovered energy, and T is the simulation time.
The discharge energy was calculated using Equation 16:

$$E_{dis} = \int_0^T max\,(0, P_{batt}\,(t))dt \quad [16]$$

where E_{dis} is the energy supplied by the battery during motoring operation.
The regenerative energy ratio was calculated using Equation 17:

$$\eta_{regen} = (\frac{E_{regen}}{E_{dis}}) \times 100 \quad [17]$$

where η_{regen} is the regenerative energy ratio.
The SOC variation was calculated using Equation 18:

$$\Delta SOC = SOC_{final} - SOC_{initial} \quad [18]$$

where SOC_{final} is the final state of charge and $SOC_{initial}$ is the initial state of charge. These energy-related outputs were used to evaluate battery energy-flow direction and SOC behaviour. They were not used to calculate absolute driving range, Wh/km energy consumption, or percentage range improvement in the present study.

Braking Force, Power, and Efficiency Calculation

The regenerative braking force was calculated from the electromagnetic torque and wheel radius, as shown in Equation 19:

$$F_b = \frac{T_e}{r} \quad [19]$$

where F_b is the regenerative braking force, T_e is the electromagnetic torque, and r is the wheel radius. During regenerative braking, the electromagnetic torque opposes the wheel's rotation, producing a braking effect.

The regenerative mechanical power was calculated using Equation 20:

$$P_{regen} = T_e \omega \quad [20]$$

where P_{regen} is the mechanical regenerative power, and ω is the wheel angular speed. The regeneration efficiency was calculated using Equation 21:

$$\eta_{energy} = \frac{P_{elec}}{P_{regen}} \times 100 \quad [21]$$

where η_{energy} is the regeneration efficiency, P_{elec} is the electrical power returned to the battery, and P_{regen} is the available mechanical power during regenerative braking.

The braking force, power, and efficiency calculations were used to compare feedforward and PID control. Since detailed component-level saturation and experimental validation were outside the scope of the present work, these outputs were interpreted as model-based performance indicators. The performance-output subsystem used for these calculations is shown in Figure 9. The subsystem receives angular speed, electromagnetic torque, current, and terminal voltage as inputs. It then calculates actual speed, regenerative mechanical power, electrical power, braking force, and energy efficiency.

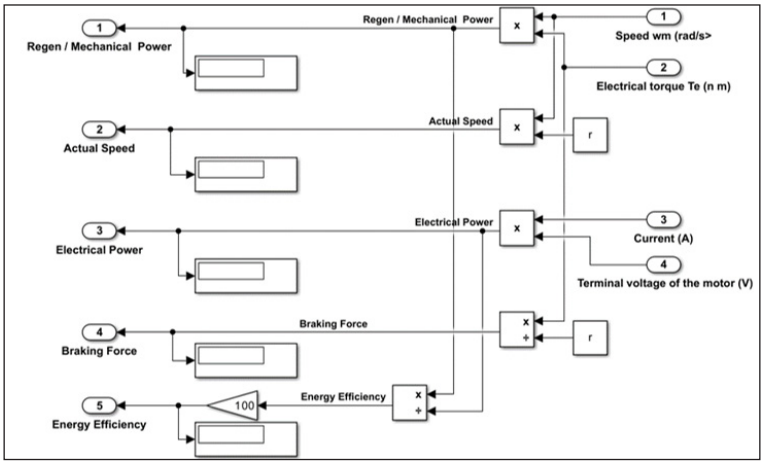

Figure 9. Performance-output subsystem for speed, torque, power, braking force, and regeneration efficiency

Model Validation Procedure

The model was validated by monitoring the mechanical and electrical responses during motoring and regenerative braking. The reference speed was compared with the actual speed to evaluate speed-tracking behaviour, while battery voltage, battery current, battery power, SOC, electromagnetic torque, angular speed, and armature current were used to verify regenerative braking operation. The validation in this study refers to internal simulation consistency and verification of regenerative braking behaviour. It does not represent experimental validation against a physical electric motorcycle prototype.

The speed-tracking error was calculated using the root mean square error (RMSE), as shown in Equation 22:

$$RMSE = \sqrt{\frac{1}{N}\sum_{i=1}^{N}(v_{ref,i} - v_i)^2} \quad [22]$$

where N is the number of samples, $v_{ref,i}$ is the reference speed at sample i, and v_i is the actual motorcycle speed at sample i.

Successful regenerative braking was identified by negative battery current during braking, opposing electromagnetic torque during deceleration, and reduced SOC drop or temporary SOC recovery during regenerative intervals. These validation outputs were used to compare the feedforward and PID-based regenerative braking responses. Therefore, the model was used to assess regenerative braking activation, controller response, and battery energy recovery trends rather than to establish final motor sizing, range extension, or hardware operating limits.

RESULT AND DISCUSSION

Force Response During Hilly-Terrain Operation

The longitudinal force response was evaluated to verify the behaviour of the electric motorcycle under downhill, flat-road, and uphill operating conditions. Figure 10 shows the rolling resistance, air resistance, slope resistance, acceleration resistance, net motoring force, net regenerative force, and regenerative braking force acting on the motorcycle.

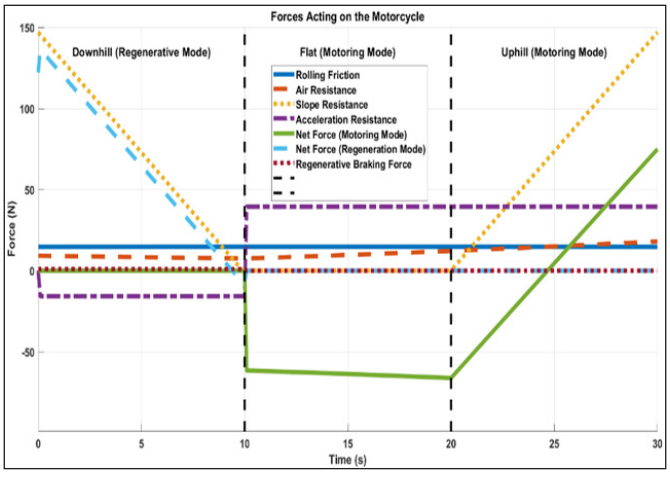

Figure 10. Forces acting on the electric motorcycle during downhill, flat-road, and uphill operation

In the downhill region from 0 s to 10 s, the slope resistance assists the motorcycle's motion. The net force in regenerative mode becomes negative, reaching approximately −60 N. This indicates that the electric machine produces an opposing braking effect as the motorcycle descends. At the same time, the regenerative braking force opposes the wheel's rotation, allowing part of the available mechanical energy to be converted into electrical energy.

In the flat-road region from 10 s to 20 s, the slope resistance is nearly absent, and the force demand becomes more stable. The motorcycle primarily needs to overcome rolling and aerodynamic resistance. In the uphill region from 20 s to 30 s, the slope resistance increases strongly, reaching approximately 75 N near the end of the profile. As a result, the required motoring force becomes positive, showing that the motor must supply additional torque to overcome the gravitational load.

This confirms that road gradient directly affects electric motorcycle energy demand. Downhill sections create an opportunity for regenerative braking, while uphill sections increase the required motoring effort. Therefore, the hilly-terrain force response supports the use of regenerative braking as an energy-recovery strategy during downhill and deceleration conditions.

Speed Tracking Under WMTC Operation

The reference and actual speed responses were compared under the WMTC-based simulation profile. Figure 11 shows the feedforward speed response, while Figure 12 shows the PID speed response.

For feedforward control, the actual speed generally follows the reference speed, but noticeable deviations occur during rapid transients. This shows that feedforward control

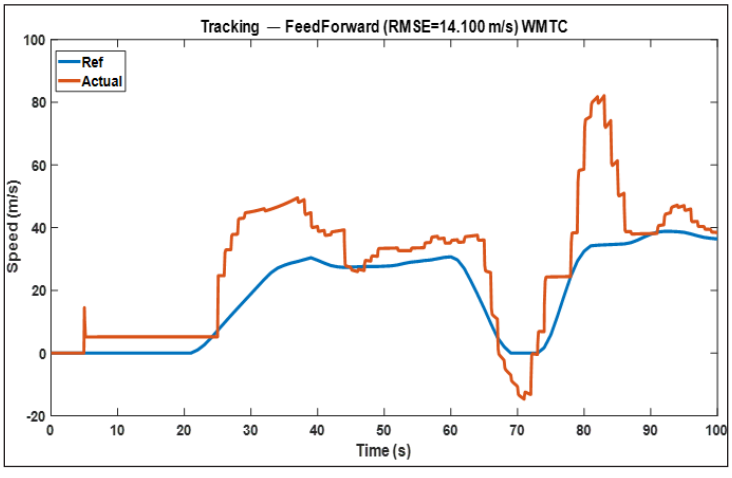

Figure 11. Reference and actual speed response using feedforward control under the WMTC profile

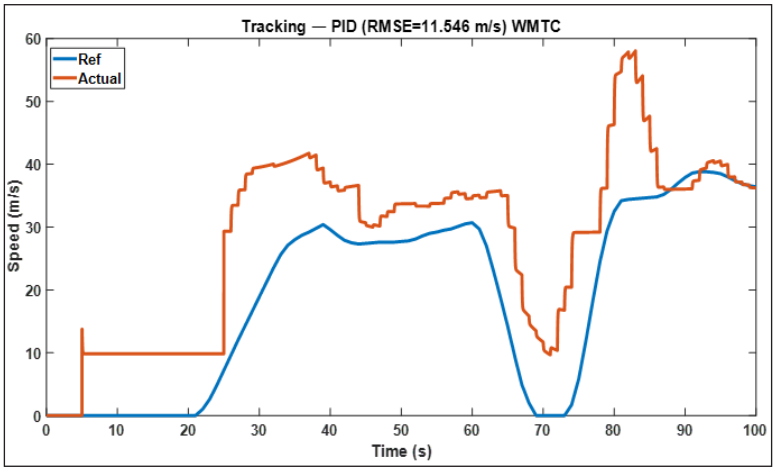

Figure 12. Reference and actual speed response using PID control under the WMTC profile

is limited under fast-transient conditions because it does not correct the speed error via feedback.

For PID control, the actual speed still deviates from the reference speed during some transient regions, but the overall tracking response is improved compared with feedforward control. The PID controller adjusts the PWM duty cycle according to the difference between the reference and actual speeds. To avoid overinterpreting transient simulated peak values as physical hardware limits, the speed response is evaluated using RMSE rather than by emphasising maximum speed values. The numerical speed-tracking comparison is shown in Table 4.

The PID controller reduced the RMSE from 14.10 m/s to 11.546 m/s. This represents an 18.1% reduction in speed-tracking error compared with feedforward control. Since RMSE measures the difference between the reference and actual speeds, a lower RMSE indicates that PID control provides better speed-tracking performance.

Table 4
WMTC Speed-Tracking Performance of Feedforward and PID Controllers

Controller	RMSE (m/s)	Tracking performance
Feedforward	14.10	Higher tracking error
PID	11.546	Lower tracking error

Battery State of Charge Response

The battery state of charge was evaluated to determine whether regenerative braking returned energy to the battery. Figure 13 shows the SOC response during motoring and regenerative braking operation.

The SOC begins at approximately 90% and decreases during motoring operation because the battery supplies electrical energy to the motor. Between approximately 60 s

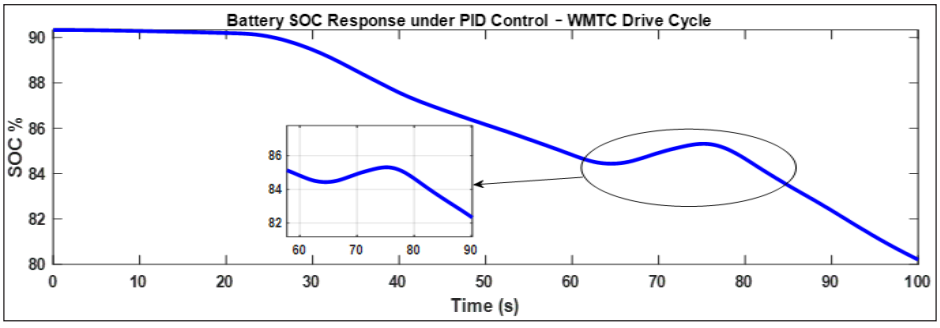

Figure 13. Battery state of charge response during motoring and regenerative braking

and 80 s, a temporary SOC recovery is observed. In this region, the SOC increases from approximately 84.5% to about 85.3%, showing that part of the braking energy is converted into electrical energy and stored back in the battery.

After the regenerative interval, the SOC decreases again as the motorcycle returns to motoring operation. By the end of the 100-second simulation window, the SOC reaches approximately 80%. This behaviour confirms that regenerative braking does not eliminate battery discharge, but it reduces the rate of depletion by recovering part of the energy during braking or downhill operation.

The SOC recovery region is important because it proves that the regenerative braking system is functioning correctly. Instead of dissipating all braking energy as heat, the system recovers a portion of the mechanical energy and returns it to the battery. Therefore, the SOC response is used as evidence of energy recovery and reduced battery depletion, not as a direct quantified driving-range improvement.

Battery Voltage, Current, and Power Response

Battery voltage, current, and power were analysed to verify the direction of energy flow during motoring and regenerative braking. Figure 14 shows the feedforward battery response, while Figure 15 shows the PID battery response.

In the feedforward case, the battery voltage, current, and power responses show alternating motoring and regenerative intervals. During motoring operation, the battery current and battery power are positive, indicating that energy flows from the battery to the motor. During regenerative braking, the battery current and battery power become negative, confirming that the direction of energy flow is reversed and that electrical energy is returned to the battery.

In the PID case, the battery current and power responses also show clear positive and negative regions. The negative current and negative power regions indicate that the DC machine operates as a generator during braking, returning energy to the battery. Compared with feedforward control, the PID response exhibits more effective regenerative charging

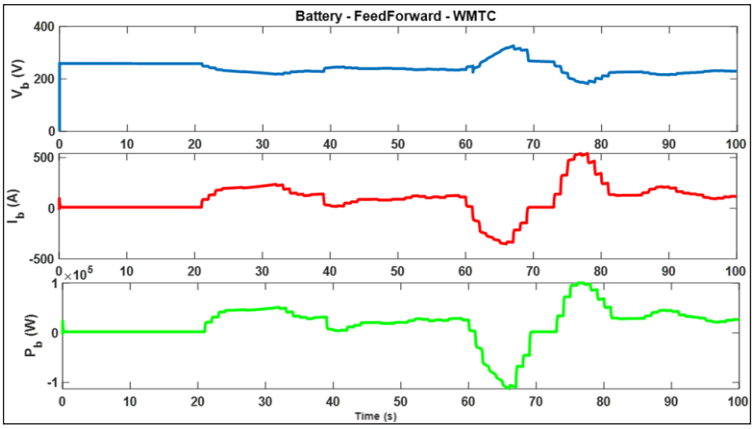

Figure 14. Battery voltage, current, and power response using feedforward control

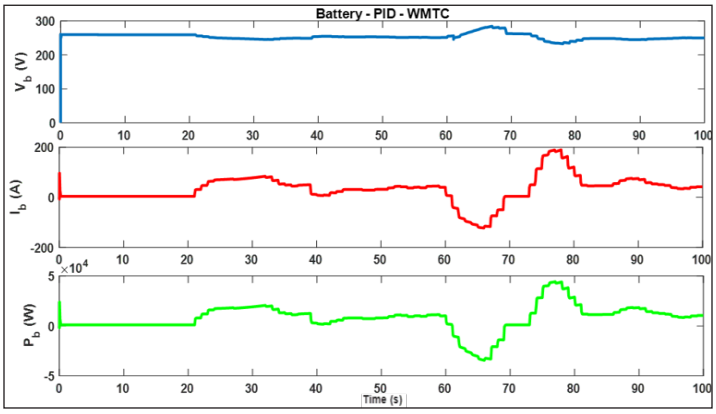

Figure 15. Battery voltage, current, and power response using PID control

behaviour, consistent with the higher recovered energy reported in Table 5. The transient battery current and power waveforms are interpreted as indicators of simulation response for energy-flow direction and controller comparison. They are not presented as experimentally validated component operating limits.

The PID controller recovered 2.20×10^5 J, while the feedforward controller recovered 1.00×10^5 J. This corresponds to a 120% increase in recovered energy. The regeneration

Table 5
WMTC Regenerative Energy and SOC Performance

Controller	Recovered energy, Eregen (J)	Regeneration fraction	SOC variation, ΔSOC (%)	Regeneration efficiency indicator
Feedforward	1.00×10^5	0.090	−13.0	0.06
PID	2.20×10^5	0.160	−10.2	0.40

fraction increased from 0.090 to 0.160, while SOC variation improved from −13.0% to −10.2%. This means the PID controller reduced SOC depletion by 2.8 percentage points compared with feedforward control.

These results show that PID control improves both battery charging behaviour and regenerative energy recovery. However, since a no-regeneration baseline was not included, the results are discussed in terms of recovered energy and SOC variation rather than absolute increase in range, Wh/km consumption, or percentage driving-range improvement.

DC Machine Torque and Current Response

The DC machine response was evaluated using angular speed, electromagnetic torque, and armature current. Figure 16 shows the feedforward response, while Figure 17 shows the PID response.

In the feedforward response, the electromagnetic torque becomes positive during motoring operation and negative during regenerative braking. The negative torque region

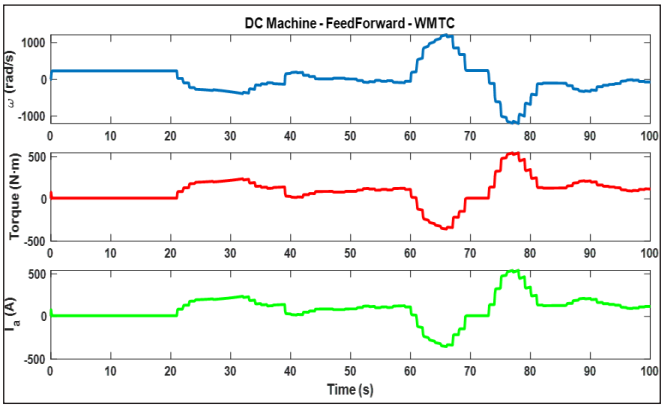

Figure 16. DC machine response using feedforward control under the WMTC profile

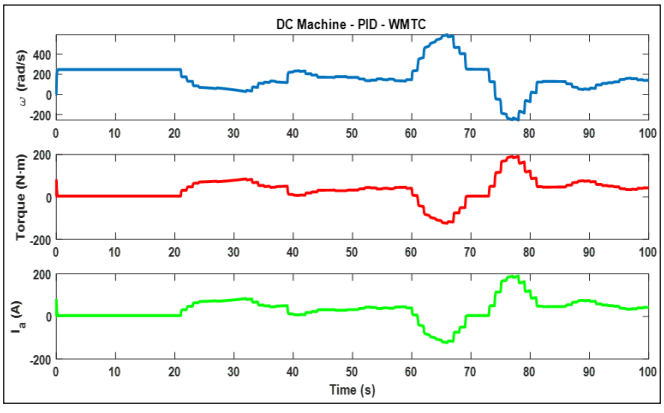

Figure 17. DC machine response using PID control under the WMTC profile

shows that the DC machine opposes the wheel motion and operates as a generator during braking. The armature current follows the torque behaviour, where the change in current direction supports the transition from motoring to regenerative operation.

In the PID response, the electromagnetic torque and armature current show a clearer transition between motoring and regenerative braking intervals. The negative torque and corresponding current reversal confirm generator operation during regenerative braking. Compared with feedforward control, PID provides a more effective regenerative response, which agrees with the higher recovered energy and lower SOC depletion reported in Table 5.

The DC machine results are used to verify the direction of torque and current flow during regenerative braking. The transient magnitudes shown in the simulation are interpreted as model-response indicators for controller comparison, while detailed motor operating limits, torque-speed constraints, current saturation, and hardware validation are outside the scope of the present study.

Integrated Performance Assessment

The results demonstrate that the proposed regenerative braking system can recover part of the mechanical energy available during downhill and deceleration conditions. The force response shows a net force of approximately −60 N during downhill operation, supporting the activation of regenerative braking. This behaviour is also reflected in the SOC response, where the battery SOC temporarily increases from about 84.5% to 85.3% between approximately 60 s and 80 s. This confirms that part of the braking energy is converted into electrical energy and returned to the battery.

The comparison between feedforward and PID control shows that PID provides better speed regulation and energy recovery. The PID controller reduced the RMSE from 14.10 m/s to 11.546 m/s, representing an 18.1% reduction in tracking error. The PID controller also increased recovered energy from 1.00×10^5 J to 2.20×10^5 J, while SOC depletion improved from −13.0% to −10.2%.

Overall, the results confirm that regenerative braking can reduce battery energy depletion during downhill and deceleration operations. The revised findings support energy recovery and SOC improvement, but they do not claim a directly quantified driving-range extension because no no-regeneration baseline, Wh/km calculation, estimated range, or percentage range improvement was included. Therefore, the present study demonstrates the energy-recovery potential of regenerative braking for electric motorcycles in hilly terrain, while direct quantification of range should be addressed in future work.

CONCLUSION

This study investigated regenerative braking as an energy-recovery strategy for electric motorcycles operating in hilly terrain. The developed model represented the transition

between motoring and regenerative braking modes by integrating longitudinal vehicle dynamics, motor-generator operation, battery response, H-bridge switching, and control operation under the WMTC driving profile.

The findings confirm that regenerative braking can return useful energy to the battery during deceleration and downhill operation. This was shown through reversed battery current, opposing electromagnetic torque, temporary SOC recovery, and reduced battery charge depletion. The comparison between feedforward and PID control also showed that controller selection directly influences both speed response and energy recovery performance. In the present simulation model, PID control outperformed feedforward control, as evidenced by lower RMSE, higher recovered energy, higher regeneration fraction, and lower SOC depletion.

The study is limited to a modelling-based evaluation, and experimental validation on a real electric motorcycle platform was not conducted. The model also focuses on longitudinal motion and does not include detailed tyre slip, rider posture variation, thermal effects, battery ageing, mechanical brake blending, hardware derating, or component-level operating limits. In addition, a no-regeneration baseline was not included; therefore, the study does not report Wh/km energy consumption, estimated driving range, or percentage range improvement.

Overall, the results show that regenerative braking can support energy recovery and reduce battery depletion in electric motorcycles operating in hilly terrain. Future work should include hardware-based validation, integration of regenerative and mechanical braking, detailed component sizing, and direct quantification of range using a no-regeneration baseline across different slope, speed, and rider-demand conditions.

ACKNOWLEDGEMENT

The authors would like to express their sincere gratitude to the Ministry of Higher Education Malaysia for supporting this research under the Fundamental Research Grant Scheme, grant number FRGS/1/2023/TK02/UIAM/01/1, entitled “Optimal Deceleration Formulation Based on Reinforcement Deep Learning for Energy Generation from Regenerative Braking Mode of an Electric Motorcycle.” The authors also acknowledge the support of the Kulliyyah of Engineering, International Islamic University Malaysia, through the KOE IIUM Engineering Merit Scholarship 2023.

REFERENCES

Aduama, P., Al-Sumaiti, A. S., & Al-Hosani, K. H. (2023). Electric vehicle charging infrastructure and energy resources: A review. *Energies, 16*(4), Article 1965. https://doi.org/10.3390/en16041965

Badran, M. A., & Toha, S. F. (2024). Employment of artificial intelligence (AI) techniques in battery management system (BMS) for electric vehicles (EV): Issues and challenges. *Pertanika Journal of Science and Technology, 32*(2), 859-881. https://doi.org/10.47836/pjst.32.2.20

Ghazali, A. K., Hassan, M. K., Radzi, M. A. M., & As'arry, A. (2020). Integrated braking force distribution for electric vehicle regenerative braking system. *Pertanika Journal of Science and Technology, 28*(Special issue 2), 173-182. https://doi.org/10.47836/pjst.28.S2.14

Heydari, S., Fajri, P., Rasheduzzaman, M., & Sabzehgar, R. (2019). Maximizing regenerative braking energy recovery of electric vehicles through dynamic low-speed cutoff point detection. *IEEE Transactions on Transportation Electrification, 5*(1), 262-270. https://doi.org/10.1109/TTE.2019.2894942

Heydari, S., Fajri, P., Sabzehgar, R., & Asrari, A. (2020). Optimal brake allocation in electric vehicles for maximizing energy harvesting during braking. *IEEE Transactions on Energy Conversion, 35*(4), 1806-1814. https://doi.org/10.1109/TEC.2020.2994520

International Energy Agency. (2022). *Global EV outlook 2022: Securing supplies for an electric future*. https://www.iea.org/reports/global-ev-outlook-2022

Joseph Godfrey, A., & Sankaranarayanan, V. (2018). A new electric braking system with energy regeneration for a BLDC motor driven electric vehicle. *Engineering Science and Technology, an International Journal, 21*(4), 704-713. https://doi.org/10.1016/j.jestch.2018.05.003

Jung, S., & Ko, J. (2021). Study on regenerative energy recovery of electric vehicle through voltage control using switched capacitor. *IEEE Transactions on Vehicular Technology, 70*(5), 4324-4339. https://doi.org/10.1109/TVT.2021.3073148

Kadav, P., & Asher, Z. D. (2019). Improving the range of electric vehicles. In *2019 Electric Vehicles International Conference (EV)* (pp. 1-5). IEEE. https://doi.org/10.1109/EV.2019.8892929

Karyatanti, I. D. P., Dewantara, B. Y., Winarno, I., Rahmatullah, D., & Nuhman. (2025). Energy management systems development in electric vehicle charging stations based on multi-source inverters with utilisation of renewable energy sources. *Pertanika Journal of Science and Technology, 33*(3), 1595-1612. https://doi.org/10.47836/pjst.33.3.22

Madichetty, S., Mishra, S., & Basu, M. (2021). New trends in electric motors and selection for electric vehicle propulsion systems. *IET Electrical Systems in Transportation, 11*(3), 186-199. https://doi.org/10.1049/els2.12018

Mohamed, M. A., Toha, S. F., Abdullah, M., Ahmad, S., Nor, K. A. M., Hassan, M. H., & Idris, A. S. (2025). Enhanced voltage regulation of buck converter-fed DC motors using fuzzy logic control under dynamic load conditions. *International Journal of Robotics and Control Systems, 5*(2), 1422-1440. https://doi.org/10.31763/ijrcs.v5i2.1836

Mohamed, M. A., Toha, S. F., Rahman, M. A., & Khairudin, M. (2025). Smart IoT energy optimisation and localisation monitoring for e-bike sharing. *IIUM Engineering Journal, 26*(2), 305-325. https://doi.org/10.31436/iiumej.v26i2.3448

Nama, T., Mondal, P., Tripathy, P., Adda, R., & Gogoi, A. K. (2022). Design, modeling and hardware implementation of regenerative braking for electric two-wheelers for hilly roads. *IEEE Access, 10*, 130602-130618. https://doi.org/10.1109/ACCESS.2022.3229597

Naseri, F., Farjah, E., & Ghanbari, T. (2017). An efficient regenerative braking system based on battery/supercapacitor for electric, hybrid, and plug-in hybrid electric vehicles with BLDC motor. *IEEE Transactions on Vehicular Technology, 66*(5), 3724-3738. https://doi.org/10.1109/TVT.2016.2611655

Podder, A. K., Chakraborty, O., Islam, S., Kumar, N. M., & Alhelou, H. H. (2021). Control strategies of different hybrid energy storage systems for electric vehicles applications. *IEEE Access, 9*, 51865-51895. https://doi.org/10.1109/ACCESS.2021.3069593

Rego, N., & Castro, R. (2023). Regenerative braking applied to a student team's electric racing motorcycle prototype: A theoretical study. *Applied Sciences, 13*(6), Article 3784. https://doi.org/10.3390/app13063784

Riczu, C., & Bauman, J. (2021). Implementation and system-level modeling of a hardware efficient cell balancing circuit for electric vehicle range extension. *IEEE Transactions on Industry Applications, 57*(3), 2883–2895. https://doi.org/10.1109/TIA.2021.3067300

Xie, Y., Wang, C., Hu, X., Lin, X., Zhang, Y., & Li, W. (2020). An MPC-based control strategy for electric vehicle battery cooling considering energy saving and battery lifespan. *IEEE Transactions on Vehicular Technology, 69*(12), 14657-14673. https://doi.org/10.1109/TVT.2020.3032989

Yang, C. (2022). Running battery electric vehicles with extended range: Coupling cost and energy analysis. *Applied Energy, 306*, Article 118116. https://doi.org/10.1016/j.apenergy.2021.118116

Yeo, W., Jung, S., Kim, S., Park, K., & Ko, J. (2020). A regenerative energy recovery system for electric vehicles charging a battery at a low speed. *Advances in Science, Technology and Engineering Systems, 5*(2), 64-73. https://doi.org/10.25046/aj050208